Free Radical Biology and Medicine 243 (2026) 126–142

Contents lists available at ScienceDirect

Free Radical Biology and Medicine

journal homepage: www.elsevier.com/locate/freeradbiomed

Hydrostatic pressure induces mitochondrial oxidative stress and mtDNA-mediated cGAS–STING activation in acute pancreatitis

Fan Chen [a], Kedong Xu [a,b], Yimin Han [a], Jiachun Ding [a], Jiaqiang Ren [a], Weikun Qian [a,b], Zheng Wang [a,b], Zheng Wu [a,b], Zhenhua Ma [a,b,*], Fang Cao [c,**]

[a] Department of Hepatobiliary Surgery, The First Affiliated Hospital of Xi'an Jiaotong University, Xi'an, 710061, China
[b] Pancreatic Disease Center of Xi'an Jiaotong University, Xi'an, 710061, China
[c] Center for Translational Medicine, The First Affiliated Hospital of Xi'an Jiaotong University, Xi'an, 710061, China

ARTICLE INFO

Keywords:
Hydrostatic pressure
Mitochondrial DNA
cGAS–STING pathway
Acinar cell injury
Acute pancreatitis

ABSTRACT

Increased mechanical pressure is a well-recognized feature of acute pancreatitis (AP), but its pathological mechanisms remain elusive. Although previous studies have emphasized shear stress-induced pancreatic injury, the effects of static hydrostatic pressure have been underappreciated. Mitochondria act as mechanosensitive organelles, and mechanical stimuli can induce mitochondrial oxidative stress. Release of mitochondrial DNA (mtDNA) could trigger activation of the cyclic GMP-AMP synthase (cGAS)–stimulator of interferon genes (STING) pathway in immune cells. However, whether increased hydrostatic pressure can induce mtDNA-mediated cGAS-STING activation in pancreatic cells is unknown. In this study, we explored the mechanistic links between pressure-induced mitochondrial dysfunction, mtDNA release, and innate immune signaling activation in AP. Acute pancreatitis was induced in mice using two models: (1) intraperitoneal injection of caerulein combined with lipopolysaccharide (LPS), and (2) retrograde infusion of methylene blue-balanced salt solution through the pancreatic duct followed by briefly clamping to mimic elevated intrapancreatic hydrostatic pressure. AR42J cells, an immortalized pancreatic adenocarcinoma cell line exhibiting acinar-like characteristics, were cultured under controlled high hydrostatic pressure conditions to investigate pressure-induced cellular responses in vitro. Elevated hydrostatic pressure markedly aggravated mitochondrial dysfunction and induced mitochondrial permeability transition pore (MPTP) opening, accompanied by increased mitochondrial ROS production, leading to mtDNA leakage and cGAS-STING pathway activation, which exacerbated inflammatory responses and AP. Inhibition of MPTP suppressed mtDNA release, reduced STING activation, and ameliorated pancreatic injury. Collectively, our data show that increased hydrostatic pressure is a critical but underappreciated mechanical insult that causes mitochondrial dysfunction and mtDNA release in pancreatic cells through MPTP opening. The associated increase in mitochondrial oxidative stress may represent a key upstream trigger in this process, and cytosolic mtDNA could subsequently activate cGAS-STING signaling and exacerbate inflammatory responses in AP. These findings suggest that mitochondrial permeability transition is a potential therapeutic target in pressure-associated AP.

1. Introduction

Acute pancreatitis (AP) presents a major medical complication because it emerges suddenly and leads to high morbidity while potentially advancing into systemic inflammatory response syndrome and multi-organ dysfunction syndrome [1]. Even with improved supportive care for severe AP, the mortality rate continues to stay between 15 % and 30 % [2]. Recent research findings show that inflammation acts as a primary pathophysiological process in AP and that inflammatory responses are closely linked to both disease severity and clinical results [3,4]. Therefore, the development of targeted therapies for AP requires a deep understanding of the molecular pathways responsible for inflammation.

Mitochondrial DNA (mtDNA) works as a powerful damage-

* Corresponding author. Department of Hepatobiliary Surgery, The First Affiliated Hospital of Xi'an Jiaotong University, Xi'an, 710061, China.
** Corresponding author. Center for Translational Medicine, The First Affiliated Hospital of Xi'an Jiaotong University, Xi'an 710061, China.
E-mail addresses: mzh@xjtu.edu.cn (Z. Ma), Lanching@xjtu.edu.cn (F. Cao).

https://doi.org/10.1016/j.freeradbiomed.2025.11.031
Received 15 September 2025; Received in revised form 14 November 2025; Accepted 16 November 2025
Available online 17 November 2025

associated molecular pattern (DAMP) which increases inflammation during AP [5,6]. Clinical studies show that patients with AP exhibit increased circulating mtDNA levels which show a positive relationship with both disease severity and organ dysfunction scores [7,8]. The release of mtDNA from pancreatic acinar cells triggers the cGAS–STING–NF-κB signaling pathway which leads to ongoing inflammation and increased pancreatic cell damage during AP [9]. When mitochondrial function becomes disrupted due to cellular stress or injury, mtDNA leaks into the cytosol for cGAS to recognize. The synthesis of cGAMP through binding activates STING. Upon activation, STING recruits TANK-binding kinase 1 (TBK1), which phosphorylates and activates the transcription factors nuclear factor-kappa B (NF-κB) and interferon regulatory factor 3 (IRF3). These transcription factors regulate the expression and secretion of type I interferons and pro-inflammatory cytokines, thereby amplifying inflammation and contributing to tissue damage [10,11]. Deletion of STING genes or its pharmacological inhibition reduces inflammation and pancreatic tissue injury in multiple animal pancreatitis models [12]. The collective results from these studies highlight the crucial role of mtDNA-STING signaling as a key driver of inflammatory processes in AP.

Pancreatic inflammation modulation by mechanical forces receives increasing recognition but scientific focus remains primarily on fluid shear force instead of hydrostatic pressure. Scientific studies extensively demonstrate how fluid shear stress affects pancreatic ductal cells by damaging epithelial barriers and triggering pro-inflammatory signaling pathways [13,14]. The early development of AP pathogenesis causes increased ductal pressure from obstruction, hypersecretion, or sphincter of Oddi dysfunction which results in elevated hydrostatic pressure that impacts pancreatic acinar cells [15,16]. Intraductal hyper NETs plays a role in the development of AP [17], but scientists have yet to fully investigate how increased hydrostatic pressure influences acinar cell inflammation and molecular pathways.

Studies indicate that cellular reactions to mechanical pressure throughout different tissues are governed by multiple mechanosensitive pathways including ion channel operations [13,14]. Mechanical stimuli trigger mechanosensory pathways to activate which leads to calcium influx that may cause mitochondrial dysfunction [18]. Hydrostatic pressure may affect pancreatic cell biology in ways that differ from fluid shear stress and other mechanical forces. Current studies have yet to confirm whether mechanosensitive pathway activation through hydrostatic pressure induces mitochondrial damage and mtDNA release in pancreatic cells. The connection between hydrostatic pressure and mitochondrial integrity in pancreatic cells have not been thoroughly investigated. The impact of pressure-induced cellular stress on mtDNA release and the subsequent cGAS-STING pathway activation in AP remains unexplored.

Our study utilized an in vitro system to examine hydrostatic pressure effect on pancreatic cells. We performed a detailed examination of how hydrostatic pressures impact mitochondrial structure and functionality, and identified the mtDNA release and the subsequent cGAS-STING signaling pathway activation. We investigated potential therapeutic strategies aimed at this specific pathway to reduce the inflammatory response induced by abnormal hydrostatic pressure. Our research reveals new insights about how hydrostatic pressure triggers inflammatory responses in acute pancreatitis which could lead to innovative treatment options for this critical condition.

2. Materials and methods

2.1. Animals

Eight-week-old male C57BL/6 J mice (weight 20 ± 1g) were purchased from Xi'an Huishi Biotechnology Co., Ltd. and were housed in individually ventilated cages in the SPF facility of the Experimental Animal Center at Xi'an Jiaotong University (four animals per cage). They were kept under controlled environmental conditions, with non-inflammatory exposure to standard laboratory food and tap water, and maintained on a regular 12/12-h light/dark cycle. Temperature was maintained at 22 ± 2 °C with humidity at 50–60 %. All animal procedures were performed in strict compliance with the guidelines and protocols approved by the Biomedical Ethics Committee of Health Science Center of Xi'an Jiaotong University (No. XJTUAE2024-2145). Before the experiments, the mice were acclimatized to the environment for one week.

2.2. Induction of acute pancreatitis in mice

To establish a model of severe acute pancreatitis in mice as a positive control, we first administered an intraperitoneal injection of caerulein (10 μg/ml) at a dosage of 50 μg/kg once every hour for a total of ten times. Following the final injection of caerulein, a single intraperitoneal injection of lipopolysaccharide (LPS) (5 mg/ml) at a dosage of 10 mg/kg was administered immediately.

Retrograde pancreatic duct injection of methylene blue-balanced salt solution was employed to simulate the high-pressure environment of the pancreatic duct in vivo. Methylene blue serves as a visual tracer to confirm successful cannulation and injection into the pancreatic ductal system. The mice were anesthetized with 2 % isoflurane inhalation, and the skin was prepared and disinfected, followed by the placement of a sterile drape. A midline incision approximately 1–1.5 cm long was made on the abdominal wall to access the abdominal cavity. The abdomen was exposed, and the duodenum was identified and flipped over to reveal the bile-pancreatic duct on the hepatic side of the duodenum. The duodenum was secured with traction sutures. One hand held the puncture needle at an angle with the tip facing upwards, penetrating through the intestinal wall until reaching the papilla, and entering the pancreatic duct by 2–3 mm. A 30-gauge needle was used to minimize tissue trauma while ensuring adequate flow. A micro clamp was used to secure the puncture needle to prevent it from dislodging. The microinjection pump was employed to infuse the methylene blue-balanced salt solution at a flow rate of 4.8 ml/h for 5 min. Throughout the infusion process, saline was used to keep the intestine moist, and the appearance of the pancreatic duct and pancreas was monitored. Distinct from conventional methods, our model involved briefly clamping the pancreatic duct for 2 min after retrograde injection, aiming to enhance the exposure of the pancreas to increased hydrostatic pressure and create a more robust pressure-induced injury model. Mice were euthanized at 24 h post-surgery by isoflurane inhalation followed by cervical dislocation, in accordance with institutional animal ethics guidelines.

Based on the experimental design and modeling protocols, the mice were randomly divided into the following four groups: NC group (normal control group, untreated mice), Sham group (mice subjected to laparotomy and pancreatic duct puncture without infusion), AP-caerulein group (mice receiving intraperitoneal injections of caerulein), and AP-pressure group (mice subjected to retrograde pancreatic duct injection of a balanced salt solution (4.8 mL/h for 5 min), followed by temporary pancreatic duct occlusion to simulate elevated intrapancreatic hydrostatic pressure).

2.3. Cell culture

The AR42J cell line, an immortalized pancreatic adenocarcinoma cell line that shares similarities with pancreatic acinar cells, was purchased from Procell. The cells were cultured in Ham's F-12K medium supplemented with 20 % fetal bovine serum at a temperature of 37 °C and a humidity of 5 % CO_2.

2.4. Pressure chambers

Two square pressure chambers, crafted from aluminum alloy with internal dimensions of 13.5 cm × 9.5 cm × 1.5 cm, were constructed to fit within a standard 37 °C, 5 % CO_2, 95 % air incubator (Fig. 4A). Each

chamber contained two racks to hold cell culture plates. Water was placed at the bottom of each chamber to generate a humid environment. A remote humidity/temperature monitor (VWR) was used to verify that internal conditions matched the incubator's settings (37 °C, 95 % relative humidity). Reservoir water levels were checked post-experiment and every other day during extended experiments, with no significant reduction observed in either the reservoirs or the media covering the cells. A separate trial confirmed stable humidity levels, consistent with incubator conditions, throughout multi-day experiments. A gas cylinder containing a 5 % CO_2/21 % O_2/balance N_2 mixture was stationed outside the incubator, fitted with a dual-stage, ultra-low-pressure regulator. Chamber pressure was monitored using digital pressure gauges in the outlet line, ensuring pressure remained above standard atmospheric pressure as per the pressure monitoring table. Miniature needle valves in the inlet and outlet lines maintained a steady gas flow rate (~0.1 ml/min, or ~0.005 % of chamber volume/min) to regulate pressure and support airflow during experiments.

2.5. Cell experimental procedure

Cells were routinely seeded and incubated overnight to allow adherence. Subsequently, the cell plates were transferred to the pressure chambers and cultured under pressures of 40 kPa or 80 kPa above atmospheric pressure (designated as the 40 kPa and 80 kPa groups, respectively). In contrast, control group cells were maintained at atmospheric pressure (NC group). The duration of pressure exposure varies based on the specific experimental protocols. The pressures of 40 and 80 kPa were selected based on preliminary optimization experiments, as lower pressures (<20 kPa) did not consistently induce measurable mitochondrial or inflammatory responses in AR42J cells. Cells were maintained under standard culture conditions (37 °C, 5 % CO_2, atmospheric O_2) throughout the experiments. Pressure chambers were flushed with the same incubator gas mixture to maintain comparable O_2 tensions between control and pressurized groups.

2.6. Measurement of intracellular Ca^{2+} under hydrostatic pressure

Intracellular Ca^{2+} levels were monitored using the fluorescent probe Fluo-4 AM (Beyotime, China). AR42J cells were incubated with 5 μM Fluo-4 AM for 30 min at 37 °C to allow dye loading and subsequently washed once with HBSS. Cells were then subjected to hydrostatic pressures of 40 kPa or 80 kPa using the customized pressure chamber, while control cells were maintained at atmospheric pressure. Fluorescence intensity (excitation 488 nm, emission 525 nm) was recorded by a microplate reader at 5, 10, 20, 30, 60, and 90 s after pressure application. Baseline fluorescence (F_0) was defined as the mean intensity at 0 s prior to pressurization. Relative fluorescence (F/F_0) was calculated for each time point to normalize inter-well variability. Relative fluorescence was normalized to the baseline value (0 s) and expressed as F/F_0 to depict early-phase Ca^{2+} influx kinetics under hydrostatic stress.

2.7. Histopathological analysis

24 h after modeling, the mice were euthanized, and their pancreatic tissues were fixed in 4 % paraformaldehyde for 48 h, followed by dehydration and embedding. The paraffin-embedded tissue sections, 5 μm in thickness, were deparaffinized and stained with hematoxylin and eosin. The degree of pancreatic edema, inflammation, hemorrhage, and necrosis was examined under an optical microscope. A standard immunohistochemistry (IHC) protocol was used for staining pancreatic tissues. In brief, the samples were blocked and incubated overnight at 4 °C with primary antibodies against cGAS (HUABIO, HA500023, 1:500), STING (Selleck, F2884, 1:2000), pTBK1 (Affinity, AF8190, 1:100), and pIRF3 (Affinity, AF2436, 1:100). Subsequently, the sections were washed three times with phosphate-buffered saline (PBS) and incubated with a horseradish peroxidase (HRP)-conjugated secondary antibody at 37 °C for 20 min. Finally, after color development with DAB, the sections were counterstained with hematoxylin. The staining intensity was scored as follows: 0 for negative, 1 for weak positive, 2 for positive, and 3 for strong positive. The extent of staining was scored as: 1 point for ≤25 %, 2 points for 26–50 %, 3 points for 51–75 %, and 4 points for >75 %. The final IHC score was obtained by multiplying the intensity score by the extent of staining score [19].

2.8. Flow cytometry

To assess the infiltration levels of serum macrophages and neutrophils in model mice, PerCP Anti-Mouse CD11b Antibody (Elabscience, E-AB-F1081F) and anti-mouse F4/80 Antibody (Biolegend, QA17A29) were used to detect serum macrophages. FITC Anti-Mouse CD11b Antibody (Elabscience, E-AB-F1081C) and PE Anti-Mouse Ly6G Antibody (Elabscience, E-AB-F1108D) were utilized to evaluate the infiltration levels of neutrophils in serum. The percentage of mouse serum macrophages and neutrophils was quantified using the NovoCyte Flow Cytometer (Agilent, CA, USA).

2.9. Measurement of cytokines, amylase, and lipase

After successful modeling, blood samples were collected from the periorbital region of the mice. The blood samples were stored at 4 °C overnight and then centrifuged at 3000 rpm for 15 min to obtain serum. AR42J cells were cultured in six-well plates and subjected to pressure intervention (40 kPa and 80 kPa) for 24h, after which cell supernatants were collected. Serum and cell supernatant levels of cytokines (IL-1β, IL-6, TNF-α) and serum amylase (AMS) and lipase (LPS) were quantified using the Mouse IL-1β ELISA Kit (Proteintech, KE10003), Mouse IL-6 ELISA Kit (Proteintech, KE10007), Mouse TNF-α ELISA Kit (Proteintech, KE10002), Amylase Assay Kit (Nanjing Jiancheng Bioengineering Institute, C016-1-1), and Lipase Assay Kit (Nanjing Jiancheng Bioengineering Institute, A054-1-1) according to the instructions provided with the kits.

2.10. RNA extraction and quantitative real-time PCR (qRT-PCR)

Total RNA was extracted from mouse pancreatic tissues and AR42J cells using the Trizol method (Takara) to measure the expression levels of different genes. Mice pancreatic tissues homogenized with 1 mL Trizol reagent or 1 x 10^6 AR42J cells were lysed with 1 mL Trizol reagent by pipetting up and down. The samples were then subjected to the same procedure for phase separation, RNA precipitation, and washing and resuspended in RNase-free water. The purity (A260/A280: 1.8–2.0) and integrity of the total RNA samples were determined by NanoDrop and agarose gel electrophoresis. The qRT-PCR was performed on cDNA prepared from 1 μg RNA using a High-Capacity cDNA Reverse Transcription Kit (Takara) [9]. The PCR reaction mixture contained SYBR Green Master Mix, target-specific primers, and 1 μl cDNA with GAPDH as the endogenous reference, and was incubated under the standard cycling conditions (95 °C for 30 s, 43 cycles of 95 °C for 5 s and 59.5 °C for 30 s) on a real-time PCR machine (Bio-Rad CFX-96). No-template and no-reverse-transcriptase controls were included to ensure the specificity of the reactions. All experiments were conducted in triplicate. The target gene primers were listed in Table 1.

2.11. Detection of extracellular and circulating mtDNA by droplet digital PCR (ddPCR)

Cell culture supernatants and mouse sera were collected after hydrostatic pressure exposure. Samples were centrifuged at 3000×*g* for 10 min to remove debris, and DNA was isolated using a plasma/serum DNA isolation kit (Abcam, USA). The concentration of mitochondrial DNA (mtDNA) was quantified by droplet digital PCR (ddPCR) using a QX200 Droplet Digital PCR System (Bio-Rad, USA). PCR reactions were

Table 1
The target gene primers.

Gene	Primer sequences (5′-3′)
mouse-IL-1β-F	TGTAATGAAAGACGGCACACC
mouse-IL-1β-R	TCTTCTTTGGGTATTGCTTGG
mouse-IL-6-F	CAAAGCCAGAGTCCTTCAGA
mouse-IL-6-R	GATGGTCTTGGTCCTTAGCC
mouse-TNF-α-F	GCCTCTTCTCATTCCTGCTTG
mouse-TNF-α-R	CTGATGAGAGGGAGGCCATT
mouse-STING-F	TCGCACGAACTTGGACTACTG
mouse-STING-R	CCAACTGAGGTATATGTCAGCAG
mouse-cGAS-F	GTCGGAGTTCAAAGGTGTGGA
mouse-cGAS-R	GACTCAGCGGATTTCCTCGTG
mouse-actin-F	GTGACGTTGACATCCGTAAAGA
mouse-actin-R	GCCGGACTCATCGTACTCC
mouse-mt-ND1-F	GAGCCTCAAACTCCAAATACTCACT
mouse-mt-ND1-R	GAACTGATAAAAGGATAATAGCTATGGTTACTTCA
mouse-mt-ND2-F	ACCTACCCTATCACTCACACTAGCA
mouse-mt-ND2-R	GAGGCTCATCCTGATCATAGAATG
mouse-mt-CO3-F	CCTCGTACCAACACATGATCTAGG
mouse-mt-CO3-R	AGTGGGACTTCTAGAGGGTTAAGTG
mouse-mt-DLOOP-F	AATCTACCATCCTCCGTGAAACC
mouse-mt-DLOOP-R	TCAGTTTAGCTACCCCCAAGTTTAA
rat-IL-1β-F	ACCTTCCAGGATGAGGACATGA
rat-IL-1β-R	CTAATGGGAACGTCACACACCA
rat-IL-6-F	ATGAACTCCTTCTCCACAAGCGC
rat-IL-6-R	GGGAAGGCAGCAGGCAACAC
rat-TNF-α-F	TCAAAGGGGAACGGACATAG
rat-TNF-α-R	ACCAGGATTCTGTGGCAATC
rat-GAPDH-F	TGTTCGTCATGGGTGTGAAC
rat-GAPDH-R	ATGGCATGGACTGTGGTCAT
rat-STING-F	TCTGACTGTGAGAGCAAGCAG
rat-STING-R	ACCTTTAGGTCCCAGGCCATT
rat-cGAS-F	ACATGGCGGCTATCCTTCTCT
rat-cGAS-R	GGGTTCTGGGTACATACGTGAAA
rat-mt-ND1-F	GCCGCCCGATGATACCCATGGCCAACCTCC
rat-mt-ND1-R	GTCGACTAGGTTTGAGGGGGAATGCTG
rat-mt-ND2-F	GCCGGCCGATGATAAACTTCGCCTTAATT
rat-mt-ND2-R	GTCGACATTCGGTTCAGTCTAATCCTT
rat-mt-DLOOP-F	AAATTCTAGGCTATATACAACTAC
rat-mt-DLOOP-R	GCTAGCATGTTTATTTCTAGGC

prepared with ddPCR Supermix for Probes (Bio-Rad) following the manufacturer's protocol, using primers specific for the mtCO3, mtDloop, mtND1 and mtND2 gene. Droplets were generated with a QX200 droplet generator and thermally cycled under standard conditions (95 °C for 5 min, followed by 40 cycles of 95 °C for 30 s and 56 °C for 1 min, with a final step at 90 °C for 2 min). Data were analyzed using QuantaSoft software (Bio-Rad), and mtDNA concentrations were expressed as copy numbers per microliter of supernatant or serum.

2.12. Western blotting

Mouse pancreatic tissue lysates and cell lysates were prepared using RIPA lysis buffer (Proteintech, Cat No. PR20001) with protease inhibitor and phosphatase inhibitor. Samples were homogenized with ultrasonic cell crusher and then centrifuged at [specify speed, e.g., 12,000×*g*] for 15 min at 4 °C, and the supernatants were collected to extract soluble proteins. Protein concentrations were determined using a BCA Protein Assay Kit (Proteintech, Cat No. PK10026). Equal amounts of proteins were subjected to SDS-PAGE and transferred to a PVDF membrane, followed by blocking with 5 % bovine serum albumin (BSA) in TBST for 1 h at room temperature. Primary antibodies against cGAS (HUABIO, HA500023, 1:500), STING (Proteintech, 66680-1-Ig, 1:5000), TBK1 (Affinity, DF7026, 1:1000), pTBK1 (Affinity, AF8190, 1:1000), IRF3 (Affinity, DF6895, 1:1000), pIRF3 (Affinity, AF2436, 1:1000), MPO (Proteintech, 22225-1-AP, 1:1000), CD206 (Proteintech, 32647-1-AP, 1:1000), SDHA (Proteintech, 14865-1-AP, 1:10000), PHB1 (Proteintech, 10787-1-AP, 1:5000), and VDAC1 (Proteintech, 55259-1-AP, 1:2000) were incubated with the PVDF membrane overnight at 4 °C. The membrane was then washed with TBST 5 times, and incubated with HRP-conjugated secondary antibody for 1 h at room temperature. Protein bands were visualized by Bio-Rad ChemiDoc MP Chemiluminescent Gel Imaging System. All experiments were repeated in triplicate.

2.13. Mitochondrial membrane potential assay

Mitochondrial membrane potential in primary acinar cells isolated from model mice and AR42J cells was measured using JC-1 (Thermo Fisher Scientific, Waltham, MA, USA, Cat No. T3168) and TMRM (Thermo Fisher Scientific, Waltham, MA, USA, Cat No. I34361) dyes. Cells were stained according to the manufacturer's instructions, with 2 μg/mL JC-1 or 100 nM TMRM and incubated for 30 min at 37 °C in a 5 % CO_2 atmosphere. Cells were washed with PBS and subjected to flow cytometry (Agilent, CA, USA) to measure fluorescence ratios (JC-1: red/green; TMRM: fluorescence intensity) and laser confocal microscopy (Leica TCS SP5 II, Wetzlar, Germany) to visualize mitochondrial staining. Each sample type was performed in triplicate with unstained cells or CCCP-treated cells as a depolarized control.

2.14. Mitochondrial permeability transition pore (MPTP) assay

AR42J cells were cultured in a pressure chamber at 40 kPa or 80 kPa for 24 h to induce stress, with or without Cyclosporin A (CsA) (TargetMol, 59865-13-3, 5 μg/mL) to inhibit MPTP opening. Experimental groups included: (1) Ctrl (normal control), (2) Ctrl + CsA (normal culture with CsA), (3) 40 kPa (cells at 40 kPa), (4) 40 kPa + CsA (cells at 40 kPa with CsA), (5) 80 kPa (cells at 80 kPa), and (6) 80 kPa + CsA (cells at 80 kPa with CsA). The opening of MPTP was detected using a Mitochondrial Permeability Transition Pore Assay Kit (Thermo Fisher Scientific, USA, Cat No. I35103) according to the manufacturer's protocol. In brief, the cells were stained with the supplied fluorescent dyes (calcein-AM and $CoCl_2$) and incubated at 37 °C for 15 min in a 5 % CO_2 incubator. After washing with HBSS, the stained cells were subjected to flow cytometry analysis to quantify the fluorescence intensity and laser confocal microscopy to visualize MPTP activity. Experiments were performed in triplicate for each group, with fluorescence intensity of calcein-AM indicating MPTP opening.

2.15. Mitochondrial and double-stranded DNA (dsDNA) staining and detection

Cytoplasmic free mtDNA was measured in the supernatants of AR42J cells or in supernatants of the primary acinar cells isolated from the model mice. To quantify the amount of mtDNA, a dsDNA Quantitation Reagent, PicoGreen (Thermo Fisher Scientific, USA, Cat No. P11495), was used according to the manufacturer's instructions. PicoGreen reagent as a 200 × concentrated stock solution in anhydrous DMSO (100 μL) was equilibrated to room temperature. To prepare a working solution, the 200 × concentrated PicoGreen reagent was diluted in 1 × TE buffer (10 mM Tris-HCl, 1 mM EDTA, pH 7.5, 1:200) on the day of the experiment.

Supernatants from cells were obtained by centrifugation at (1000×*g* for 5 min), then stained with 1 × PicoGreen working solution (1 mL), and incubated at 37 °C for 1 h in the dark. Subsequently, fluorescence was read in a microplate reader (SPARK, Tecan, Austria) at excitation/emission wavelengths of 480/520 nm. The resulting fluorescence intensity is proportional to the concentration of dsDNA in the sample. The stained cells were examined using the Leica LAS X laser confocal microscope to confirm the localization of mtDNA.

2.16. Electron microscopy detection

Pancreas samples from normal and model mice were immediately fixed in 1.5 mL of electron microscopy fixative (2.5 % glutaraldehyde in 0.1 M cacodylate buffer, pH 7.4) at 4 °C for 24 h. Following 24 h of pressure intervention (40 kPa or 80 kPa), AR42J cells were

enzymatically digested and centrifuged at 800 rpm for 10 min to collect cell aggregates. The cell pellets were suspended with 1.5 mL of electron microscopy fixative and centrifuged again at 800 rpm for 5 min. This resuspension-centrifugation step was repeated twice.

Tissues and cells were fixed, dehydrated, embedded, sectioned and stained. Mitochondria ultrastructure was observed by imaging on a transmission electron microscope (Hitachi HT-7800). Representative images were captured for qualitative assessment.

2.17. Statistical analysis

Statistical analysis was conducted using GraphPad Prism version 10.1.2. Quantitative data are expressed as mean ± standard error of the mean (SEM). One-way and Two-way analysis of variance (ANOVA) was employed to compare values among three groups; comparisons between two groups were performed using independent samples *t*-test or rank-sum test. A p-value <0.05 was considered statistically significant (*p < 0.05, **p < 0.01, ***p < 0.001, ****p < 0.0001).

3. Results

3.1. Establishment of the mouse model of AP via retrograde pancreatic duct injection

The in vivo mouse model of AP via retrograde pancreatic duct injection was established to explore the possible role of hydrostatic pressure in AP. A balanced salt solution was injected retrogradely into the pancreatic duct at a constant flow rate of 4.8 mL/h for 5 min to construct the pressure-induced AP mouse model and to investigate the role of high hydrostatic pressure in the development of AP (Fig. 1A). The sham-operated animals underwent laparotomy with pancreatic duct puncture, but without fluid injection. To further strengthen the role of hydrostatic pressure during the induction of pancreatitis, transient occlusion of the pancreatic duct was performed immediately after retrograde pancreatic infusion. In addition to these model groups, AP was also induced by a classical caerulein-based model as a positive control. Caerulein (50 μg/kg) was administered intraperitoneally every hour for a total of ten injections followed by a single injection of LPS (10 mg/kg) after the last injection of caerulein (Fig. 1B). As shown in Fig. 1C, the pancreatic tissues of mice subjected to intrapancreatic hypertension appeared severely damaged and necrosis of pancreatic acinar cells and inflammatory cell infiltration (histology was performed with HE staining) when compared to the normal control group. In accordance with histopathology, serum AMS and LPS levels were determined by ELISA and showed significantly higher in AP model groups compared with the control (Fig. 1D). Flow cytometry analysis showed a significant increase of peripheral blood Mø and NE in the AP groups compared with normal mice, (Fig. 1F and G). The expression levels of CD206 (macrophage marker) and MPO (neutrophil marker) were significantly increased in the pancreatic tissues of AP mice (Fig. 1H). In addition, the expression levels of pro-inflammatory cytokines such as IL-1β, IL-6, and TNF-α were also significantly upregulated in serum and pancreatic tissues of the model mice (Fig. 1E–I). The above-mentioned findings indicate that the pressure-induced AP mouse model was successfully established with specific histological damage and inflammation.

3.2. Mitochondrial damage and mitochondrial DNA release in pressure-induced AP

Pancreatic tissues from mice were collected for transmission electron microscopy (TEM) examination 24 h after retrograde pancreatic duct injection. As shown in Fig. 2A, TEM analysis revealed severe mitochondrial swelling, partial destruction of cristae and formation of autophagosomes in the AP-caerulein and AP-pressure groups, suggesting obvious mitochondrial injury. JC-1 staining showed that the mitochondrial membrane potential in primary pancreatic acinar cells from AP modeled mice was significantly depolarized, compared with that in the control groups (Fig. 2B). Moreover, western blotting analysis was performed to further verify mitochondrial injury. The results showed that compared with the control and sham groups, the protein levels of mitochondrial markers, including SDHA, PHB1 and VDAC1 were significantly decreased in pancreatic tissues of mice in the AP-caerulein and AP-pressure groups (Fig. 2C, D, E, H). Serum levels of dsDNA were measured by a fluorescence microplate reader to preliminarily assess the release of mtDNA into the circulation. The AP modeled group had significantly higher serum dsDNA levels than the control and sham groups (Fig. 2F). RT-qPCR analysis of pancreatic tissues revealed the upregulated transcription levels of mtCO3, mtDloop, mtND1 and mtND2 in the AP-caerulein and AP-pressure groups, which suggested mtDNA accumulated (Fig. 2G). To clarify the release of mtDNA into the circulation in AP modeled mice, absolute quantification of circulating mtDNA in peripheral serum was performed by droplet digital PCR (ddPCR). The results showed a significant serum mtDNA increase in the AP-pressure group (Fig. 2I). These results indicated that retrograde pancreatic duct injection and transient ductal hypertension caused mitochondrial injury in pancreatic acinar cells and promoted the release of mtDNA into the circulation. The increased release of mtDNA suggests that mtDNA may act as DAMPs entering the circulation, exacerbating the inflammatory response.

3.3. Activation of the cGAS-STING signaling pathway in pancreatic tissue of mice with pressure-induced AP

Mitochondrial DNA release was observed to be enhanced under high hydrostatic pressure condition, the possibility of the involvement of cGAS–STING pathway in pressure-induced AP was further investigated. In response to cytosolic double-stranded DNA, such as mtDNA, the cytosolic DNA sensor cGAS is activated, which results in the production of cGAMP to further activate STING and promote inflammatory responses. Immunohistochemical detection of cGAS and STING proteins in the pancreatic tissues of model mice was performed. The results indicated that both the AP-caerulein group and the AP-pressure group showed a significant increase in the expression of cGAS and STING proteins after modeling, and the downstream proteins of STING, phosphorylated TBK1 (pTBK1) and phosphorylated IRF3 (pIRF3), also exhibited a significant increase in expression (Fig. 3A–E).Western blotting analysis demonstrated that the protein levels of cGAS and STING were significantly increased in the pancreas of mice with pressure-induced AP (Fig. 3F–H). Consistently, their transcript levels were also significantly increased, as determined by RT-qPCR (Fig. 3I and J). We further determined the levels of cGAMP, the enzymatic product of cGAS, in the pancreas and found that it was significantly increased, which directly demonstrated the activation of cGAS-STING pathway (Fig. 3N). In addition, the downstream effector proteins of STING pathway, pTBK1 and pIRF3, were also found to be significantly increased (Fig. 3K–M).

3.4. Elevated hydrostatic pressure induces inflammatory-like changes in cultured AR42J cell line in vitro

Our investigation into whether hydrostatic pressure can trigger inflammatory responses in vitro required the creation of a custom high-pressure culture chamber for pressurizing AR42J pancreatic-derived cells (Fig. 4A). To investigate the effects of varying hydrostatic pressures on cellular growth states, AR42J cells were cultured under hydrostatic pressures of varying degrees (0 kPa, 10 kPa, 20 kPa, 40 kPa, and 80 kPa) above standard atmospheric pressure for 24h, 48h, and 72h. The CCK-8 assay demonstrated that the growth curve of cells exposed to a pressure exceeding 40 kPa and 80 kPa above standard atmospheric pressure was significantly inhibited (Fig. 4B). Our subsequent assays will utilize 40 kPa and 80 kPa since the results indicated these pressures should be tested further. Morphological examination by light microscopy showed that exposure to 80 kPa had a slight observed impact on

cell morphology, with a subtle more-rounded shape, in comparison to the control cells, while cells exposed to 40 kPa exhibited no discernible morphological changes (Fig. 4C). No apparent cell death was observed under the applied conditions. The levels of the enzymes AMS and LPS in the cell culture supernatant were also significantly increased after exposure to the high hydrostatic pressure (Fig. 4D and E), which are widely accepted markers for injury in pancreatic cells. In addition, RT-qPCR analyses further revealed that the high hydrostatic pressure

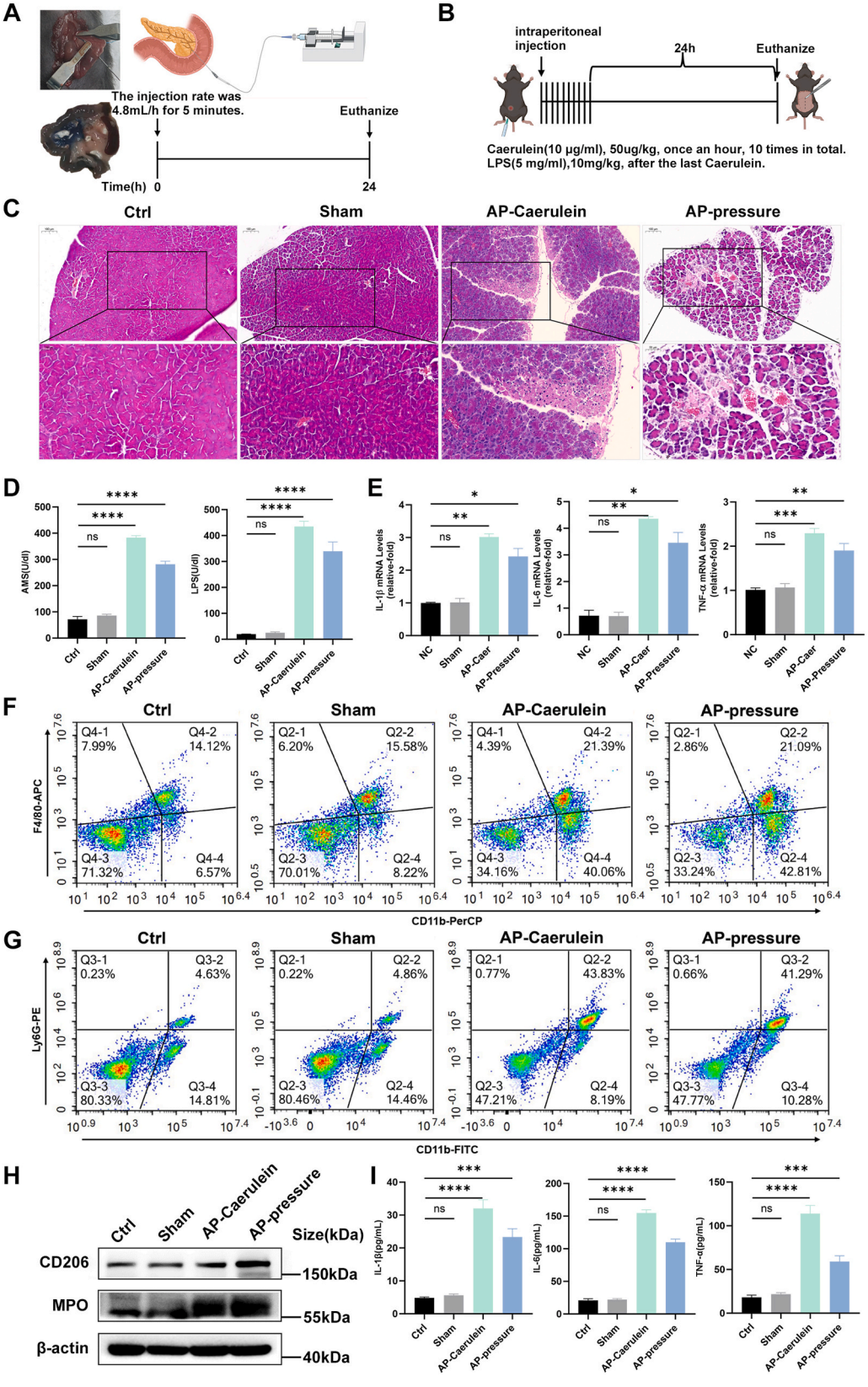

(caption on next page)

Fig. 1. Establishment of the acute pancreatitis mouse model.
A, B Schematic diagram of the acute pancreatitis mouse modeling. The AP-pressure group received a continuous infusion of balanced salt solution at a rate of 4.8 mL/h for 5 min via retrograde cannulation of the bile-pancreatic duct (**A**); the Sham group underwent a sham surgery with only laparotomy and pancreatic duct cannulation; AP-Caerulein group was subjected to intraperitoneal injection of caerulein in mice to create a model (**B**) (n = 6). **C** H&E staining images to observe the extent of pancreatic tissue damage and inflammatory infiltration in the model mice (scale bar, 100 μm and 50 μm). **D** Serum amylase (AMS) and lipase (LPS) levels in model mice after 12 h. **E** RT-qPCR detection of the levels of inflammatory factors IL-1β, IL-6, and TNF-α in the pancreatic tissue of model mice (n = 6). **F, G** Flow cytometry analysis of serum macrophage (Mø) and neutrophil (NE) abundance in model mice. **H** Increased protein levels of CD206 and MPO in model mice (n = 3). **I** ELISA detection of serum inflammatory factors IL-1β, IL-6, and TNF-α levels (n = 6). All data are presented as means, and all error bars represent the standard error of the mean (SEM). *p < 0.05, **p < 0.01, ***p < 0.001, ****p < 0.0001.

exposure resulted in a significant increase of the pro-inflammatory cytokine transcripts IL-1β, IL-6, and TNF-α in AR42J cells (Fig. 4F–H). The increase in cytokine levels in cell culture supernatants aligns with the observed transcriptional data (Fig. 4I–K). Our data showed that hydrostatic pressure alone evokes an inflammatory-like response in AR42J cells, which supports the hypothesis that mechanical forces elicit an early pro-inflammatory signal cascade in pancreatic cells.

3.5. Elevated hydrostatic pressure exposure causes mitochondrial dysfunction and oxidative stress changes

Given the inflammation induced by hydrostatic pressure and the well-established role of mitochondrial dysfunction in promoting inflammatory response, mitochondrial integrity and function were assessed to identify potential causative pathways. As shown in Fig. 5A, TEM showed that high hydrostatic pressure treatment induced obvious mitochondrial swelling and cristae shrinkage and dissolution. Notably, the 80 kPa treated cell group were observed to exhibit more obvious endoplasmic reticulum expansion, along with the formation of autophagosomes and myelin-like bodies. These results suggested that exposure to increased hydrostatic pressure for 24 h may cause ultrastructural changes in mitochondria. Subsequently, flow cytometry was used to detect intracellular ROS levels for further evaluating the impact of hydrostatic pressure on oxidative stress. In both DCFH- and DHE-stained cells, the mean fluorescence intensity (MFI) was increased under pressure interventions (Fig. 5B and C). Additionally, mitochondrial ROS levels evaluated using MitoSox Green staining also showed abnormal hydrostatic pressure treatment induced a certain increase in mitochondrial ROS (Fig. 5D).

To evaluate intracellular Ca^{2+} dynamics under hydrostatic stress, AR42J cells were loaded with the fluorescent probe Fluo-4 AM and exposed to 0 kPa (control), 40 kPa, or 80 kPa for 5–90 s. Control cells exhibited minimal fluctuations around baseline throughout the observation period. In contrast, cells exposed to 40 kPa displayed a biphasic response characterized by an initial nadir at 10 s, followed by a rapid overshoot at 20 s and sustained mild elevation through 90 s. Notably, the 80 kPa group demonstrated an inverse early response, with a transient peak at 10 s followed by gradual decline (Fig. 5E). Two-way ANOVA revealed a significant main effect of time [$F(5,90) = 5.281$, $P = 0.0003$], no significant main effect of pressure [$F(2,90) = 1.545$, $P = 0.2189$], but a highly significant time × pressure interaction [$F(10,90) = 18.29$, $P < 0.0001$]. These findings demonstrate that hydrostatic pressure elicits pressure-specific temporal patterns of Ca^{2+} signaling rather than producing uniform elevation across all conditions. Specifically, moderate pressure (40 kPa) triggers a dip-then-rebound pattern, whereas high pressure (80 kPa) induces a transient spike, consistent with mechanosensitive, pressure-dependent Ca^{2+} signaling dynamics. In addition to this early response, a significant elevation was detected 24 h after sustained pressure exposure in intracellular Ca^{2+} levels (Fig. 5F), coinciding with mitochondrial depolarization and activation of downstream signaling pathways. Together, these findings suggest that hydrostatic pressure induces a biphasic Ca^{2+} response: an immediate transient influx reflecting mechanical stimulation, and a delayed accumulation associated with persistent mitochondrial dysfunction and stress signaling.

Additionally, there was a noticeable decrease in ATP levels within the AR42J cells following the pressure intervention (Fig. 5G). Furthermore, the mitochondrial membrane potential was detected by JC-1 and TMRM assays. As shown in Fig. 5H and I, JC-1 staining showed an increase in the monomer form (green fluorescence) and a decrease in the polymer form (red fluorescence), leading to an elevated green/red fluorescence ratio in the 40 kPa and 80 kPa groups. The increased green/red fluorescence intensity ratio indicated mitochondrial depolarization (Fig. 5H). Consistent with the results in Fig. 5H, TMRM staining indicated a diminished mitochondrial fluorescence signal under pressure exposure, confirming the loss of mitochondrial membrane potential (Fig. 5I). Collectively, these findings provide clear evidence that exposure to elevated hydrostatic pressure induces mitochondrial morphological disruption, oxidative stress, and mitochondrial dysfunction in AR42J pancreatic cells.

3.6. Mitochondrial DNA release and activation of the cGAS-STING signaling pathway in AR42J cells under pressure culture conditions

mtDNA is a well-known activator of the cGAS–STING signaling pathway. Our research examined mtDNA function to establish how high hydrostatic pressure activates the innate immune response. The presence and localization of mtDNA were determined under pressure conditions. Picogreen staining followed by confocal microscopy analysis showed a strong cytoplasmic dsDNA signal at 24 h and 48 h of hydrostatic pressure treatment (Fig. 6A and B). The dispersed extranuclear bright fluorescence spots (white arrows) suggested the release of mtDNA into the cytosol. The quantification of dsDNA content by a fluorescence plate reader also revealed a significant increase in the amount of dsDNA in the culture supernatant from cells treated with hydrostatic pressure (Fig. 6C), which was indicative of the enhanced release of mtDNA outside of the cells. Moreover, a significant increase in the level of mtDNA in the cell culture medium supernatant (reflecting extracellular release), including mtCO3, mtDloop, mtND1, and mtND2 transcripts, was also detected by ddPCR specific for mtDNA under pressure conditions (Fig. 6D). These data suggested that high hydrostatic pressure induces mitochondrial dysfunction and the release of mtDNA. Besides, both the cGAS and STING protein levels were found to be significantly upregulated after hydrostatic pressure treatment (Fig. 6E and F). In addition, their mRNA expression levels were also significantly increased (Fig. 6G). The levels of phosphorylated TBK1 (pTBK1), the upstream kinase of IRF3, and phosphorylated IRF3 (pIRF3), the downstream molecule of the cGAS–STING signaling pathway, were also significantly increased under pressure conditions (Fig. 6H and I). Immunofluorescence staining also showed that the expression levels of cGAS and pIRF3 were increased with cytoplasmic localization, which was consistent with the biochemical results (Fig. 6J and K). These results suggested that exposure to non-physiological high hydrostatic pressure induces mitochondrial damage, which in turn causes the release of mtDNA. Accumulation of mtDNA further activates the cGAS–STING signaling pathway and downstream proinflammatory signaling.

3.7. Pressure-induced MPTP opening promotes mtDNA release and activation of the cGAS-STING pathway

The opening status of mitochondrial permeability transition pore (MPTP) was examined to determine its role in high hydrostatic pressure-

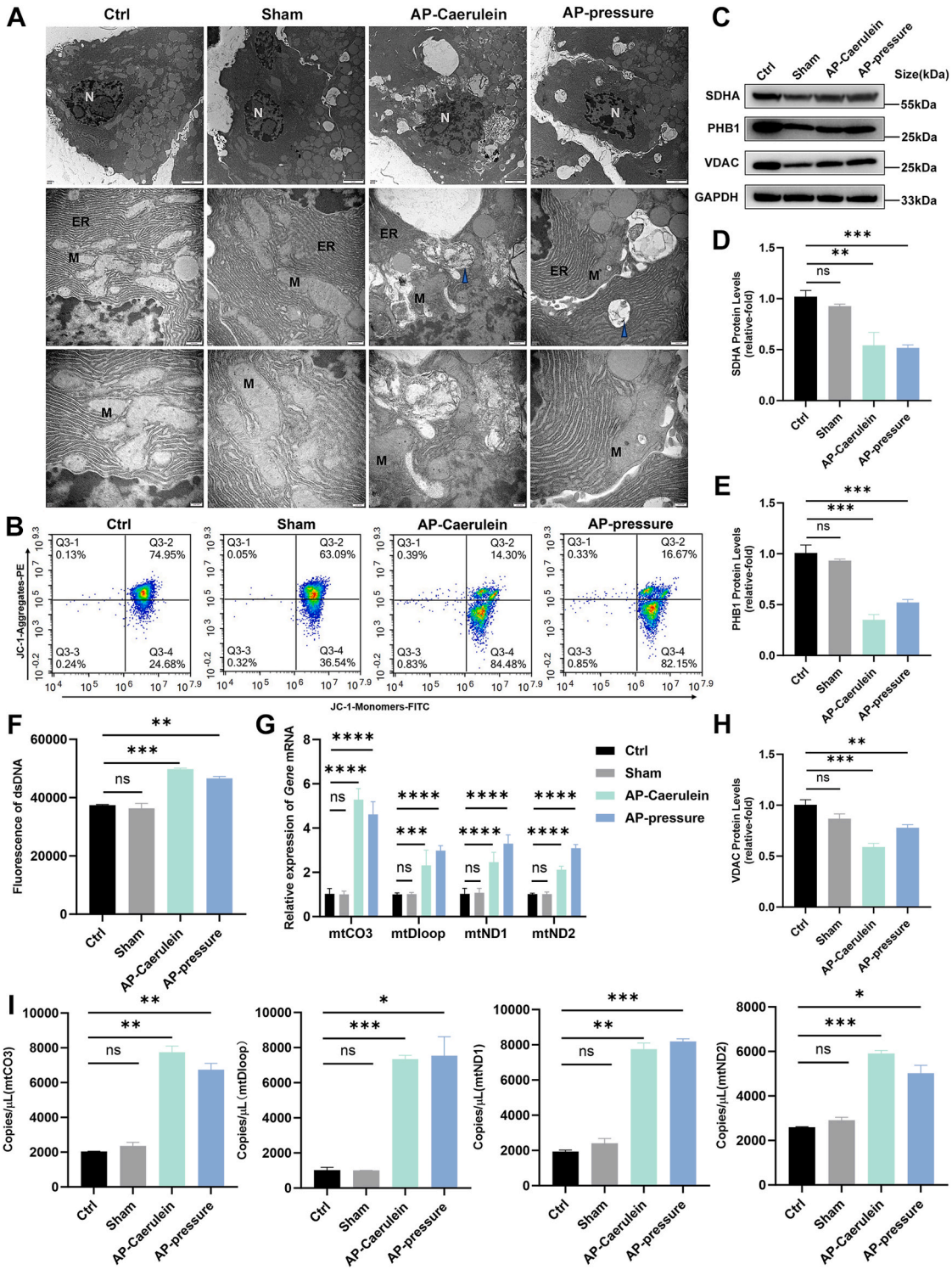

Fig. 2. Mitochondrial damage and the release of mitochondrial DNA (mtDNA) in acinar cells of mice with pressure-induced pancreatitis.
A Electron microscopy images of pancreatic tissue from different treatment groups of mice; Ctrl, normal control group; Sham, sham surgery group; AP-Caerulein, the positive control group modeled with caerulein; AP-pressure, the experimental group with retrograde pancreatic duct injection (scale bars: 2 μm, 500 nm, and 200 nm). ER, endoplasmic reticulum; M, mitochondria; blue small triangles indicate autophagosomes. **B** Flow cytometry analysis of JC-1 staining to detect changes in mitochondrial membrane potential in primary acinar cells from modeled mice. Mitochondrial membrane potential depolarization was observed in acinar cells from both the AP-Caerulein and AP-pressure groups. **C** Downregulation of SDHA(**D**), PHB1(**E**), and VDAC(**H**) protein levels in pancreatic tissue of mice with pressure-induced pancreatitis (n = 3). **F** Picogreen staining showed a significant increase in serum double-stranded DNA (dsDNA) levels in model mice (n = 6). **G** RT-qPCR analysis revealed a significant increase in mtDNA levels at the mRNA level in the pancreatic tissue of model mice (n = 6). **I** Digital PCR (ddPCR) analysis indicated an increase in mtDNA copy number in the serum of mice subjected to retrograde pancreatic duct injection (n = 6). All data are presented as means, and all error bars represent the standard error of the mean (SEM). *$p < 0.05$, **$p < 0.01$, ***$p < 0.001$, ****$p < 0.0001$. (For interpretation of the references to color in this figure legend, the reader is referred to the Web version of this article.)

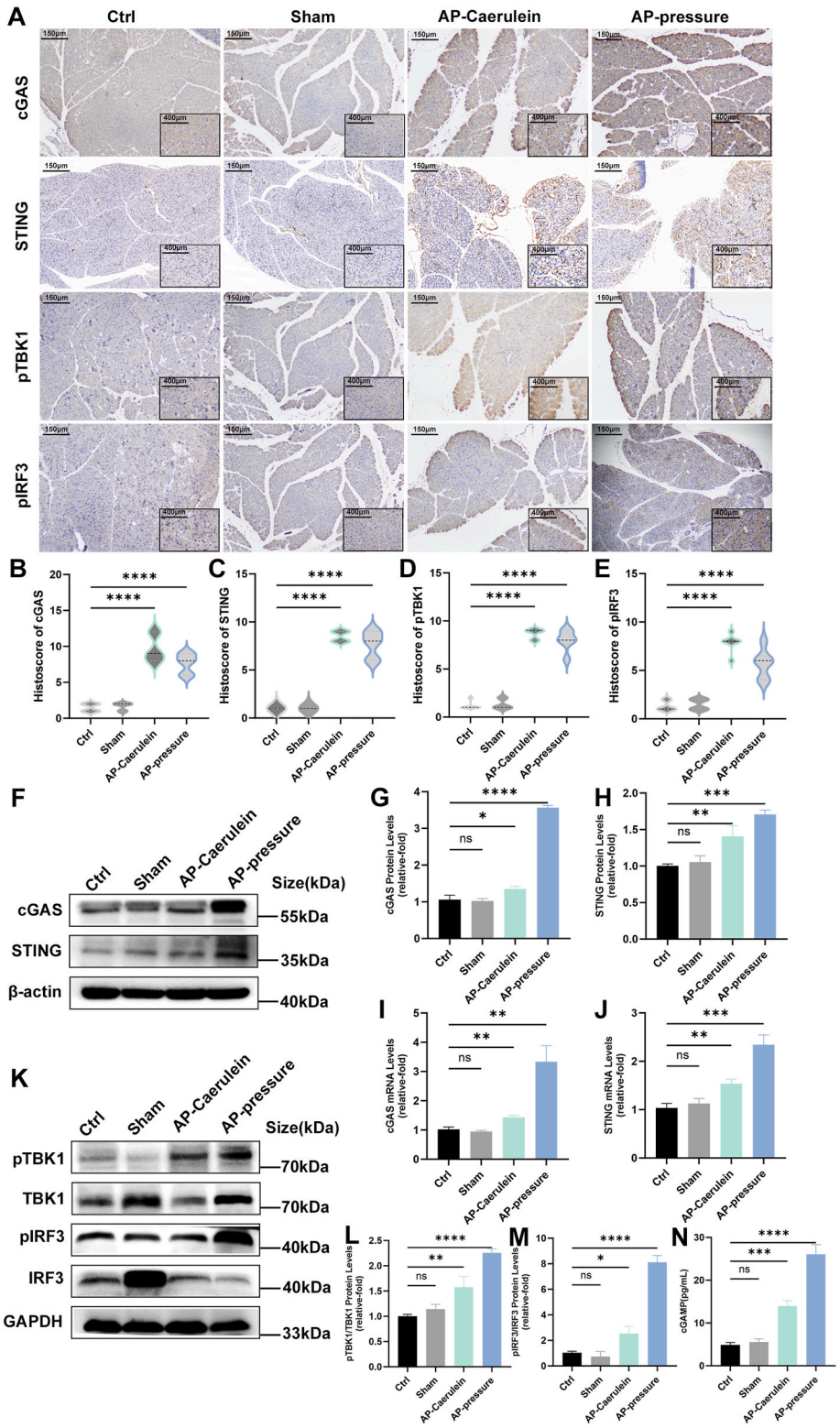

Fig. 3. Activation of the cGAS-STING signaling pathway in pancreatic tissue of mice with pressure-induced pancreatitis.
A Immunohistochemical staining of pancreatic tissue for cGAS, STING, pTBK1, and pIRF3 proteins in mice with pressure-induced pancreatitis (n = 6). **B-E** Pathological scores for the immunohistochemical staining for the expression levels of cGAS (**B**), STING (**C**), pTBK1 (**D**), and pIRF3 (**E**). **F-H** Upregulation of cGAS and STING protein levels in pancreatic tissue of mice with pressure-induced pancreatitis (n = 3). **I, J** RT-qPCR detection of upregulated cGAS and STING mRNA levels in pancreatic tissue of model mice. **K-M** Activation of downstream molecules of STING in pressure-induced pancreatitis. Upregulation of pTBK1 (**L**) and pIRF3 (**M**) protein levels (n = 3). **N** ELISA detection of increased serum cGAMP levels in model mice. The data are presented as mean values, with all error bars indicating the standard error of the mean (SEM). *p < 0.05, **p < 0.01, ***p < 0.001, and ****p < 0.0001.

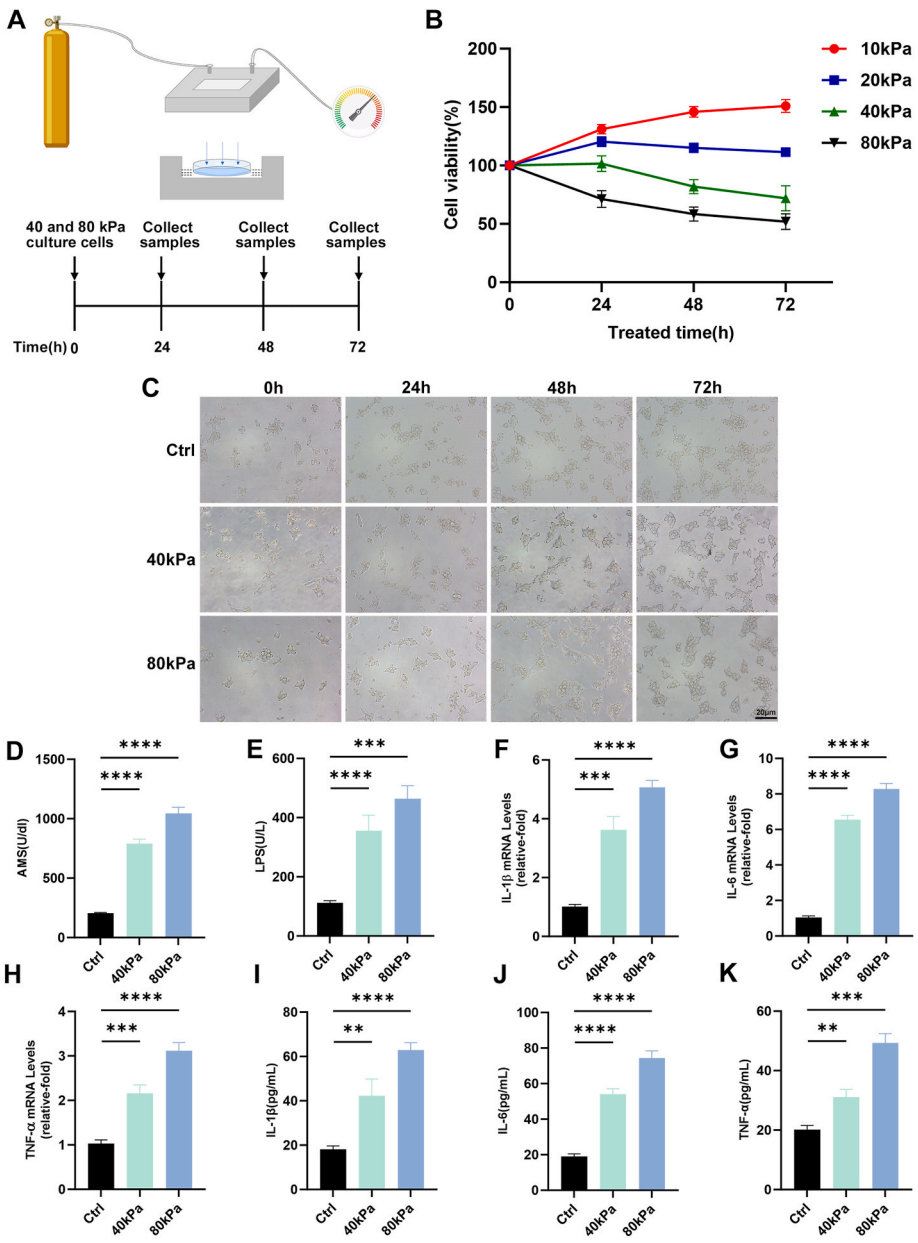

Fig. 4. Pressure culture of AR42J cells in vitro induces inflammatory-like changes.
A The in vitro pressure intervention device and the flow chart of the high-pressure intervention on cells. The immortalized rat pancreatic exocrine cell line AR42J was utilized for the intervention culture. Cells in the experimental group were subjected to varying pressures (40 kPa and 80 kPa) for 24 h, while cells in the control group were maintained under normal conditions. **B** CCK8 proliferation assay to detect cell proliferation under pressure intervention (n = 6). **C** Morphological changes in AR42J cells after pressure intervention were observed using bright-field optical microscopy. Cells cultured at 80 kPa pressure exhibited slight morphological alterations, appearing rounder than those maintained under normal atmospheric pressure, although no significant cell death was noted. **D, E** The levels of amylase (AMS) and lipase (LPS) in the culture supernatant of cells were also significantly elevated following pressure intervention (n = 6). **F-H** RT-qPCR analysis revealed a significant increase in the mRNA levels of the inflammatory cytokines IL-1β, IL-6, and TNF-α in cells subjected to pressure intervention (n = 6). **I-K** ELISA analysis demonstrated a marked elevation in the levels of IL-1β, IL-6, and TNF-α in the supernatant of the cell culture medium following pressure intervention (n = 6). The data are presented as mean values, with all error bars indicating the standard error of the mean (SEM). *p < 0.05, **p < 0.01, ***p < 0.001, and ****p < 0.0001.

induced cytosolic mtDNA accumulation. As shown in Fig. 7A, AR42J cells exposed to 40 kPa or 80 kPa hydrostatic pressure for 24 h exhibited significantly increased MPTP opening. When cells were pre-treated with the MPTP inhibitor CsA, this effect was markedly attenuated (Fig. 7B). These findings indicated that mechanical stress-induced mitochondrial permeability resulted, at least in part, from MPTP activation. Our next step was to establish the involvement of MPTP in mtDNA release. Measurement of dsDNA concentration in the cytosolic fraction and supernatant revealed a significant increase in mtDNA amount following exposure to pressure, and this was considerably decreased when cells were treated with CsA (Fig. 7C–E). To examine if this process is involved in the innate immune activation, we determined the status of cGAS–STING signaling. Western blot analysis indicated that pressure induced an increase in the expression levels of cGAS, STING, and their downstream molecules pTBK1 and pIRF3, and this effect was markedly attenuated in CsA-treated cells (Fig. 7F–J). Additionally, the expression levels of typical inflammatory cytokines including IL-1β, IL-6, and TNF-α were also significantly decreased following treatment with MPTP inhibitor, at both the transcriptional and protein levels (Fig. 7K and L).

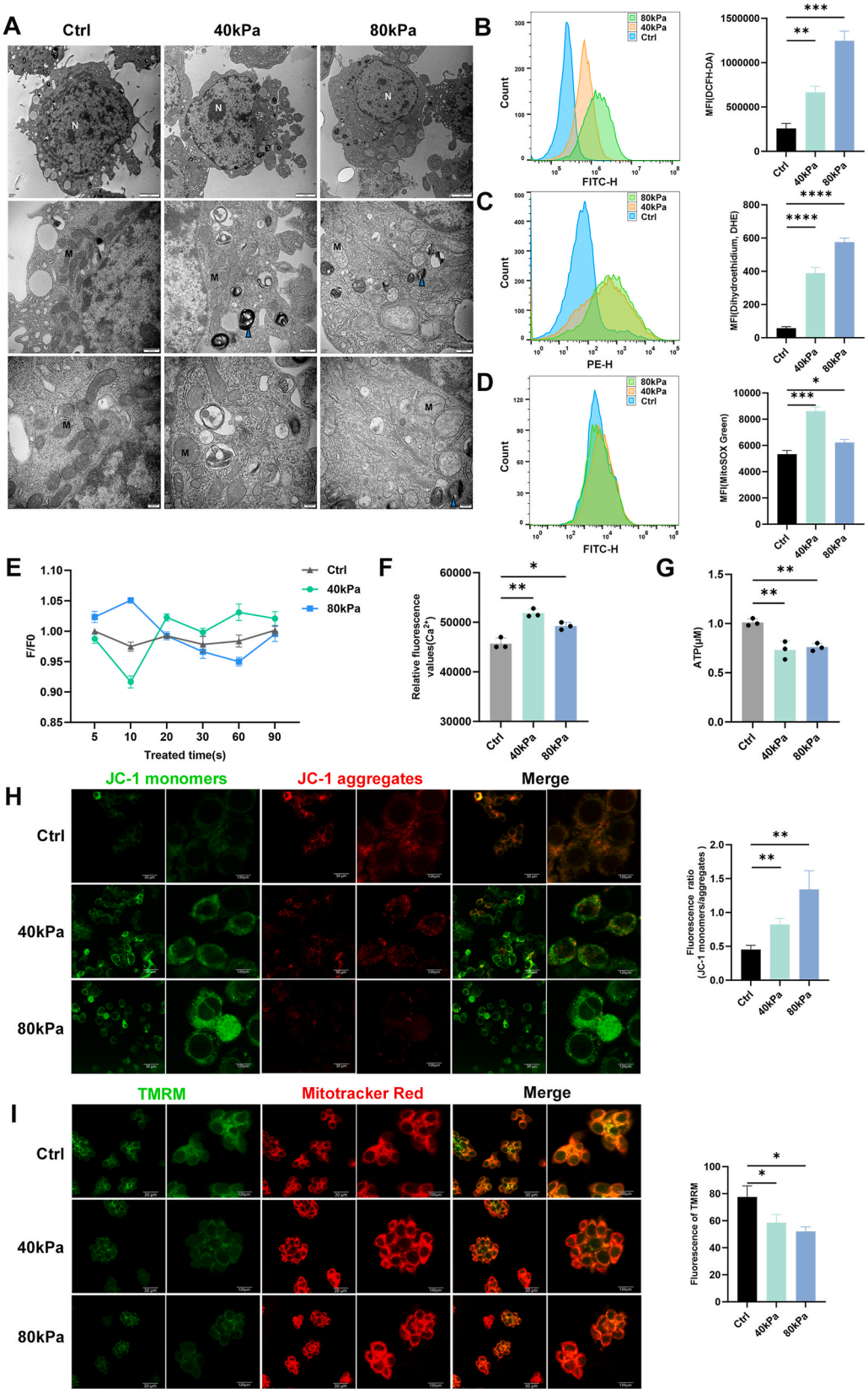

(caption on next page)

Fig. 5. Pressure culture induces mitochondrial damage and oxidative stress changes in AR42J cells.
A Electron microscopy images depict acinar cell mitochondria subjected to various pressure interventions (scale bars: 2 μm, 500 nm, and 200 nm). Following pressure intervention, mitochondrial cristae are absent, and mitochondrial matrix swelling is evident. M, mitochondria; N, nucleus; and small blue triangles signify autophagosomes. **B, C** Post-pressure intervention in AR42J cells, DCFH and DHE staining, assessed via flow cytometry, reveals elevated intracellular ROS levels and a notable increase in the mean fluorescence index (MFI). **D** MitoSox Green staining of AR42J cells, followed by flow cytometry, demonstrates an increase in mitochondrial ROS production, as indicated by MFI. **E** Fluo-4 AM-based detection of early Ca^{2+} responses in AR42J cells under 0 kPa, 40 kPa and 80 kPa hydrostatic pressure. Relative fluorescence (F/F_0) was measured 5–90 s after pressurization, showing transient Ca^{2+} fluctuations. Values represent mean ± SEM (n = 6). **F** Fluo-4 AM fluorescence probe detection showed that after 24 h of pressure intervention, the Ca^{2+} levels in AR42J cells were significantly elevated (n = 3). **G** After 24 h of pressure intervention, the ATP levels in the AR42J cells significantly decreased (n = 3). **H** JC-1 staining, observed via confocal microscopy, indicates depolarization of the mitochondrial membrane potential in AR42J cells after 24 h of pressure intervention (scale bar, 30 μm). **I** Tetramethylrhodamine (TMRM) staining, also viewed through confocal microscopy, reveals alterations in the depolarization of the mitochondrial membrane potential in AR42J cells after 48 h of pressure intervention (scale bar, 30 μm). The data are presented as mean values, with all error bars indicating the standard error of the mean (SEM). *p < 0.05, **p < 0.01, ***p < 0.001, and ****p < 0.0001. (For interpretation of the references to color in this figure legend, the reader is referred to the Web version of this article.)

4. Discussion

AP presents as a disease with rapid inflammatory onset yet its mechanisms are not well understood. Activation of innate immunity is an important early event to drive AP, which can be stimulated by a variety of factors, including mechanical stress. Accumulating evidence has suggested that physical stress, such as fluid shear stress, can disrupt the integrity of the pancreatic epithelial barriers and promote AP by activating downstream pro-inflammatory signaling [17]. The effect of hydrostatic pressure elevation on pancreatic acinar cell inflammation and how it leads to innate immune activation during AP, however, remains largely unknown. Our investigation demonstrated that elevated hydrostatic pressure in pancreas resulted in mitochondrial dysfunction followed by cytosolic mtDNA release which triggered the cGAS–STING signaling pathway and intensified inflammation during AP.

Mitochondrial dysfunction has been reported to be involved in the pathogenesis of AP. Studies have found mitochondrial dysfunction in peripheral blood mononuclear cells isolated from patients with mild AP [20]. Mitochondrial morphological changes such as fragmentation, cristae disappearance, and decreased ATP production were also observed in neuronal and retinal cell lines after exposure to high hydrostatic pressure, suggesting the vulnerability of mitochondria to mechanical stress [21,22]. Consistent with the previous study, we also found mitochondrial swelling, cristae disorganization, mitochondrial membrane depolarization, and increased ROS generation in both an in vivo mouse model of pancreatic hypertension and an in vitro pancreatic AR42J cell line abnormal hydrostatic pressure culture model. These findings indicate that high hydrostatic pressure in the pancreas could directly affect mitochondrial morphology and function and contribute to acinar cell injury.

Consistent with previous reports that fluid shear stress can rapidly alter cytosolic Ca^{2+} levels through mechanosensitive ion channels [14], we detected a rapid and transient increase in cytosolic Ca^{2+} levels within seconds of hydrostatic pressure exposure, supporting the concept that pressure acts as an acute mechanical trigger for Ca^{2+} influx in pancreatic acinar cells. Because early Ca^{2+} transients can initiate mitochondrial stress and redox imbalance that evolve over hours, subsequent analyses were conducted at 24h to assess mitochondrial dysfunction, ROS accumulation, and activation of the cGAS–STING pathway. The 24-h time point was chosen to capture the integrated cellular responses to sustained mechanical stress rather than the transient ionic events. Together, these findings suggest that an early Ca^{2+} influx serves as an initiating signal linking mechanical load to mitochondrial damage and innate immune activation in the later phase of hydrostatic pressure–induced pancreatic injury. This mechanistic connection aligns with previous evidence that pressure-induced mitochondrial depolarization and oxidative stress act upstream of mtDNA release and cGAS–STING activation.

We focused on MPTP, a non-specific channel that passes molecules less than 1.5 kDa between the matrix and the cytosol, as it has been previously reported to be associated with mtDNA release in stress-induced processes [23,24]. We found that high hydrostatic pressure led to the opening of MPTP and that inhibiting MPTP with CsA led to the reduction of mtDNA release and inhibition of the cGAS–STING signaling cascade. These results suggest that MPTP opening plays an important role in mediating mtDNA release from mitochondria to the cytosol in AP with high hydrostatic pressure.

This mechanistic link from mechanosensing through MPTP opening provides a plausible upstream pathway for the mitochondrial compromise observed under hydrostatic stress. We also observed a cytosolic accumulation of mtDNA in pancreatic cells following high hydrostatic pressure. mtDNA has been found to be an important DAMP that can trigger strong innate immune responses [25]. mtDNA has a structural and chemical resemblance to bacterial DNA and is underrepresented in methylation levels, which makes it more sensitive to oxidative damage [26–29]. The presence of ROS generation organelles and the mitochondrial matrix that is closed off from the cytosol by the mitochondrial membrane make mtDNA prone to oxidative damage [27–29]. Furthermore, high plasma mtDNA concentrations in AP patients have been shown to have a positive correlation with pancreatic necrosis and pancreatic disease outcomes [7,8]. The activation of the autophagy-lysosomal degradation pathway has been reported to contribute to the clearance of cytosolic mtDNA and the reduction of the inflammatory response and stress responses [30].

In addition to intracellular signaling, extracellular propagation of mtDNA-mediated inflammation may also occur. Moreover, mtDNA released into the extracellular space may further act as a DAMP to amplify inflammatory signaling. Circulating or secreted mtDNA can be recognized by pattern recognition receptors such as TLR9 or internalized by immune cells [31], thereby linking local cellular injury to systemic inflammatory responses. This mechanism is supported by our ddPCR results showing elevated mtDNA levels in both cell culture supernatants and mouse serum following hydrostatic pressure exposure. Such extracellular mtDNA may function in parallel with intracellular cGAS–STING activation to sustain the inflammatory milieu characteristic of acute pancreatitis. These results indicate the pro-inflammatory role of mtDNA as a DAMP during pancreatitis induced by high hydrostatic pressure. Future studies are warranted to dissect the relative contributions of extracellular versus intracellular mtDNA signaling in the progression of pressure-induced pancreatic inflammation.

The inflammatory milieu of acute pancreatitis contains multiple sources of extracellular DNA, including nuclear DNA and neutrophil extracellular traps (NETs). While we cannot fully exclude their contribution, our results support a predominant role for mtDNA: serum mtDNA levels and cytosolic mtDNA release were markedly elevated under hydrostatic pressure, and pharmacological inhibition of MPTP suppressed both mtDNA release and cGAS–STING activation. These findings suggest that mitochondrial stress is a key driver of DNA-mediated innate immune signaling in our model, although future studies will be needed to dissect the relative contributions of nuclear DNA, NET-derived DNA, and mtDNA.

Although our study focused on acinar cells as the main targets in pancreatitis, other cell types may also contribute to cGAS–STING activation. Infiltrating myeloid cells can amplify type I interferon and NF-κB

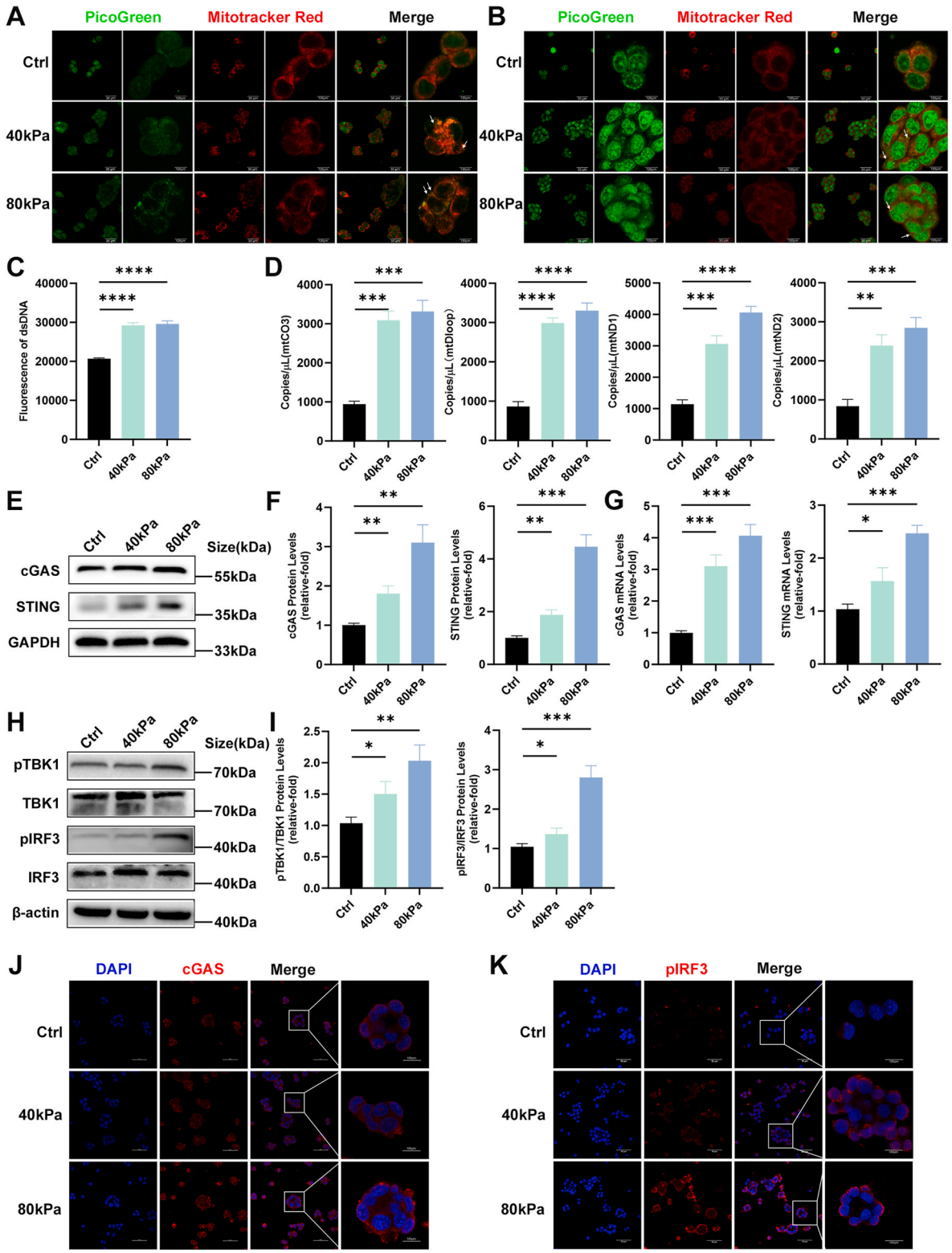

Fig. 6. Mitochondrial DNA release and activation of the cGAS-STING signaling pathway in AR42J cells under pressure culture conditions.
A, B Picogreen staining and confocal laser scanning microscopy were employed to observe mtDNA release in cells after 24 h (**A**) and 48 h (**B**) of pressure intervention (scale bar, 30 μm). **C** Detection using a fluorescence microplate reader revealed a significant increase in dsDNA levels in the cell supernatant following pressure intervention (n = 5). **D** Digital PCR (ddPCR) was utilized to assess changes in mtDNA copy number in the cell culture medium supernatant (n = 6). **E** Western blotting was performed to evaluate the protein expression of the cGAS-STING pathway (n = 3). **F, G** Both cGAS and STING were significantly upregulated at the protein and mRNA levels. **H, I** The protein levels of pTBK1 and pIRF3, which are downstream molecules of STING, were also upregulated (n = 3). **J, K** Immunofluorescence (IF) was employed to detect the protein expression of cGAS (**J**) and the downstream molecule pIRF3 (**K**) (scale bar, 50 μm). The data are presented as mean values, with all error bars indicating the standard error of the mean (SEM). *p < 0.05, **p < 0.01, ***p < 0.001, and ****p < 0.0001.

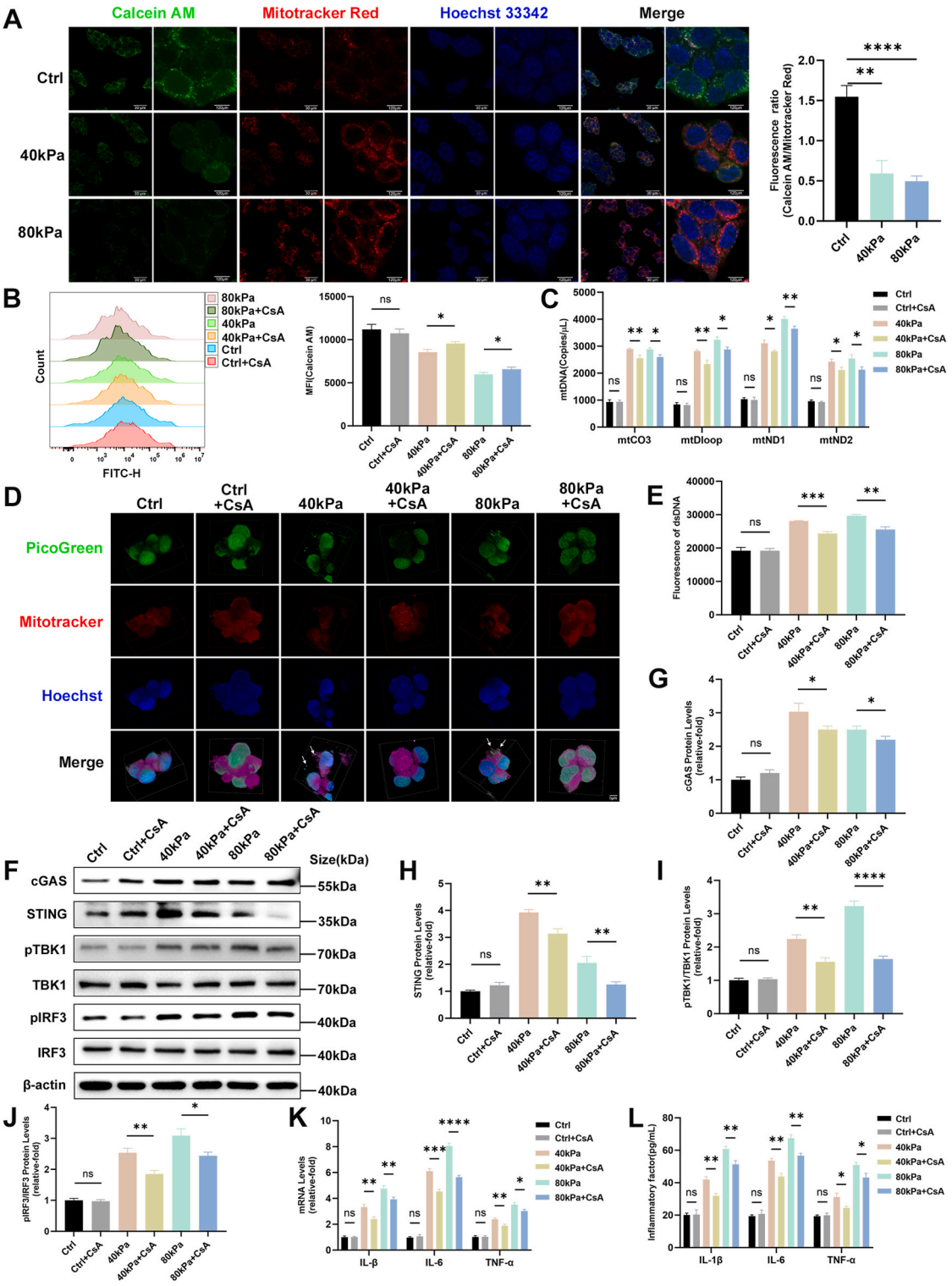

Fig. 7. Pressure-induced MPTP opening promotes mtDNA release and activation of the cGAS-STING pathway.
A The opening of the MPTP channel in AR42J cells under pressure culture conditions was observed using laser confocal microscopy with fluorescent dye (Calcein AM) staining (scale bar, 30 μm). **B** The MPTP inhibitor Cyclosporin A (CsA) reverses the pressure-induced opening of the MPTP. The extent of MPTP opening was quantified by flow cytometry and expressed as mean fluorescence intensity (MFI). **C** Changes in mtDNA copy number in the cell culture supernatant following CsA treatment. **D, E** CsA treatment resulted in a reduction of cytoplasmic mtDNA release. After CsA treatment, the release of mtDNA following stress intervention was assessed via PicoGreen staining and confocal laser scanning microscopy (**D**) (scale bar, 5 μm); the level of double-stranded DNA (dsDNA) in the supernatant of AR42J cells was measured using a fluorescence microplate reader (**E**). **F-J** CsA mitigated the pressure-induced activation of the cGAS-STING pathway, inhibiting the activation of cGAS (**G**), STING (**H**), pTBK1 (**I**), and pIRF3 (**J**) (n = 3). **K, L** CsA suppressed the pressure-induced upregulation of IL-1β, IL-6, and TNF-α (n = 6). The data are presented as mean values, with all error bars indicating the standard error of the mean (SEM). *p < 0.05, **p < 0.01, ***p < 0.001, and ****p < 0.0001.

cytokine signaling, while neuronal and glial cells may participate in neurogenic inflammation through the same pathway [31,32]. In addition, ductal epithelial cells are directly exposed to elevated luminal pressures and may undergo mitochondrial stress or release nucleic acids that further engage innate immune signaling [17,33]. These findings suggest that, under conditions of ductal obstruction or altered flow, both acinar and ductal compartments may participate in initiating or amplifying inflammatory signaling within the pancreas. While our present study was designed to delineate the effects of static hydrostatic pressure specifically in acinar cells, we acknowledge that ductal cells likely contribute to the overall inflammatory network through mechanotransduction-related mechanisms. Future studies employing cell type–specific models (such as primary ductal cell cultures, organoids, or conditional knockout approaches) will be valuable for distinguishing the relative roles of these distinct pancreatic cell populations in cGAS–STING activation under mechanical stress.

The detection of exogenous and endogenous DNA by cytosolic DNA sensors is the first step in initiating the inflammatory innate immune response [34,35]. The cGAS–STING signaling cascade is one of the main cytosolic DNA sensors. Once the cGAS–STING signaling axis is activated, it activates transcription factors, including IRF3 and NF-κB, to produce cytokines such as IL-1β, IL-6, and type I interferon to initiate inflammatory responses [36,37]. A recent study has revealed that blocking cGAS–STING signaling can reduce acute pancreatitis in mice [9,19]. Although it was found that cGAS–STING signaling was involved in AP, the stimuli for cGAS–STING signaling activation during mechanical stress-induced AP remains to be determined. The current study found increased cGAS and STING protein and mRNA levels and STING downstream signaling molecule pTBK1 and pIRF3 activation in both in vivo and in vitro models of AP with high hydrostatic pressure. This increase was associated with a release of mtDNA from the mitochondria into the cytoplasm, leading to activation of the cGAS–STING signaling cascade in AP induced by high hydrostatic pressure.

It should be noted that cGAS is capable of sensing both mitochondrial and nuclear double-stranded DNA, though the comparative kinetics of pathway activation remain incompletely characterized. Studies demonstrate that mitochondrial DNA may be more readily sensed under stress conditions due to its circular conformation, lack of protective histones, and high content of unmethylated CpG motifs [23,38,39]. Comparative analyses of cytosolic nuclear and mitochondrial DNA support the view that mtDNA contributes disproportionately to cGAS-STING activation in stress settings [40]. While our current work focuses on mtDNA, future studies should explore whether differences in binding affinity translate to distinct kinetic responses, and how these temporal dynamics may influence cGAS-STING activation in pancreatic injury.

Manometric studies in humans have reported pancreatic duct pressures in the range of ~10–30 mmHg (≈1.3–4.0 kPa) under various conditions [41,42]. Other studies in mouse models of obstructive pancreatitis have reported peak intraductal pressures up to 130 mmHg (17.3 kPa) [17]. In contrast, our in vitro experiments showed that pressures within this physiological range (<20 kPa) did not consistently induce mitochondrial dysfunction or inflammatory responses in AR42J cells. Therefore, to robustly uncover mechanistic pathways, we applied exaggerated stress conditions (40 and 80 kPa), which reliably triggered mtDNA release and cGAS–STING activation. While these values exceed physiological measurements and some reported pathological pressures, they serve as a tractable model to dissect fundamental cellular mechanisms underlying pressure-induced pancreatic injury, and we acknowledge this as a limitation of our study.

The in vivo and in vitro models used in this study have also been optimized compared to the previous studies. We employed a novel mouse model in which pancreatic duct occlusion was transient after retrograde pancreatic duct infusion with saline solution to induce ductal hypertension. This method is different from traditional pancreatic duct ligation-induced duct hypertension. Consistently, we also found an increased pancreatic injury score in this new AP mouse model by histological evaluation. In addition, we developed a novel cell culture model in which AR42J cells were cultured under high hydrostatic pressure to precisely regulate the applied pressure, allowing a clear distinction of cellular responses to mechanical stress. These improvements to the in vivo and in vitro models allow the conclusions drawn from our results to be more robust. However, we did not directly measure O_2 tension in the culture medium under hydrostatic pressure. Although the chambers were equilibrated with the same incubator gas mixture, it remains possible that pressure may subtly alter dissolved oxygen levels. Future studies using O_2-sensitive probes or controlled hypoxic conditions could clarify the role of oxygen tension in pressure-induced mitochondrial dysfunction.

5. Conclusion

In summary, we have found that high hydrostatic pressure in the pancreatic duct could lead to mitochondrial dysfunction and release of mtDNA from the mitochondria to the cytoplasm and promote the activation of the cGAS–STING signaling cascade to worsen pancreatitis inflammation. This study could be extended to explore the possible treatment options for AP. As we have found that the mitochondrial dysfunction was the early stage of AP, the treatments that target mitochondrial protection, such as maintaining the membrane potential or neutralizing the overproduced ROS, might have a potential therapeutic effect. Furthermore, as the cGAS–STING signaling cascade was also found to be involved in the development of AP, the drugs that target this signaling axis might also serve as therapeutic options for AP. Overall, we believe that our study has provided new mechanistic insights into the development of AP and will help develop new treatment options for AP.

CRediT authorship contribution statement

Fan Chen: Writing – original draft, Software, Methodology. **Kedong Xu:** Writing – review & editing, Data curation. **Yimin Han:** Methodology. **Jiachun Ding:** Validation. **Jiaqiang Ren:** Visualization. **Weikun Qian:** Funding acquisition. **Zheng Wang:** Funding acquisition. **Zheng Wu:** Writing – review & editing. **Zhenhua Ma:** Writing – review & editing. **Fang Cao:** Writing – review & editing.

Ethics approval and consent to participate

All animal procedures were performed in strict compliance with the guidelines and protocols approved by the Biomedical Ethics Committee of Health Science Center of Xi'an Jiaotong University (No. XJTUAE2024-2145).

Consent for publication

All authors read and approved the final manuscript.

Availability of data and materials

The datasets used and/or analyzed during the current study are available from the corresponding author on reasonable request.

Funding

This study was supported by the National Natural Science Foundation of China (No. 82372895); the Key Research and Development Program of Shaanxi (No. 2022SF-437, 2024SF2-GJHX-03, 2025SF-YBXM-207), the Youth Star of Science and Technology Program of Shaanxi (No. 2025ZC-KJXX-126) and the Innovative Team Foundation of Shaanxi Health Commission (No. 2024TD-16).

Declaration of competing interest

The authors declare that they have no competing interests.

Acknowledgements

The authors gratefully acknowledge the laboratory members for their continuous support.

Abbreviations

AP	Acute pancreatitis
cGAS	Cyclic GMP-AMP synthase
DAMP	Damage-associated molecular pattern
dsDNA	Double stranded DNA
mtDNA	Mitochondrial DNA
STING	Stimulator of interferon genes
IRF3	Interferon regulatory factor 3
pIRF3	Phospho-interferon regulatory factor 3
TBK1	TANK binding kinase 1
pTBK1	Phospho-TANK binding kinase 1
IL-6	Interleukin 6
IL-1β	Interleukin 1β
TNF-α	Tumor necrosis factor α
LPS	Lipopolysaccharide
IHC	Immunohistochemistry
HRP	Horseradish peroxidase
cGAMP	Cyclic GMP-AMP
CsA	Cyclosporin A
AMS	Amylase
LPS	Lipase
MPTP	Mitochondrial permeability transition pore
MFI	Mean fluorescence index
SEM	Standard error of the mean

Appendix A. Supplementary data

Supplementary data to this article can be found online at https://doi.org/10.1016/j.freeradbiomed.2025.11.031.

References

[1] P.J. Lee, G.I. Papachristou, New insights into acute pancreatitis, Nat. Rev. Gastroenterol. Hepatol. 16 (8) (2019) 479–496.
[2] N.J. Schepers, O.J. Bakker, M.G. Besselink, U. Ahmed Ali, T.L. Bollen, H. G. Gooszen, H.C. van Santvoort, M.J. Bruno, G. Dutch Pancreatitis Study, Impact of characteristics of organ failure and infected necrosis on mortality in necrotising pancreatitis, Gut 68 (6) (2019) 1044–1051.
[3] M. Sendler, C. van den Brandt, J. Glaubitz, A. Wilden, J. Golchert, F.U. Weiss, G. Homuth, L.L. De Freitas Chama, N. Mishra, U.M. Mahajan, L. Bossaller, U. Volker, B.M. Broker, J. Mayerle, M.M. Lerch, NLRP3 inflammasome regulates development of systemic inflammatory response and compensatory anti-inflammatory response syndromes in mice with acute pancreatitis, Gastroenterology 158 (1) (2020) 253–269 e14.
[4] A. Habtezion, A.S. Gukovskaya, S.J. Pandol, Acute pancreatitis: a multifaceted set of organelle and cellular interactions, Gastroenterology 156 (7) (2019) 1941–1950.
[5] A.P. West, G.S. Shadel, Mitochondrial DNA in innate immune responses and inflammatory pathology, Nat. Rev. Immunol. 17 (6) (2017) 363–375.
[6] A. Ablasser, Z.J. Chen, cGAS in action: expanding roles in immunity and inflammation, Science 363 (6431) (2019).
[7] W. Yakah, I. Shah, D. Skelton-Badlani, S.D. Freedman, Y.V. Popov, S.G. Sheth, B.A. P.W. Group, Circulating mitochondrial DNA as a diagnostic biomarker for predicting disease severity in patients with acute pancreatitis, Gastroenterology 164 (6) (2023) 1009–1011 e3.
[8] G.M. Ezzat, S.M. Nageb, M.A. Haredi, M.A. El-Masry, Mitochondrial DNA copy number, a damage-associated molecular pattern molecule, can predict pancreatic necrosis and is correlated with the severity of acute pancreatitis, Dig. Dis. Sci. 68 (11) (2023) 4175–4185.
[9] D. Zhang, J. Li, L. Zhao, Z. Yang, C. Wu, Y. Liu, W. Li, Z. Jin, J. Ma, Mitochondrial DNA leakage promotes persistent pancreatic acinar cell injury in acute pancreatitis via the cGAS-STING-NF-kappaB pathway, Inflammation 48 (3) (2025) 1420–1437.
[10] X. Zhang, X.C. Bai, Z.J. Chen, Structures and mechanisms in the cGAS-STING innate immunity pathway, Immunity 53 (1) (2020) 43–53.
[11] M. Motwani, S. Pesiridis, K.A. Fitzgerald, DNA sensing by the cGAS-STING pathway in health and disease, Nat. Rev. Genet. 20 (11) (2019) 657–674.
[12] Q. Zhao, Y. Wei, S.J. Pandol, L. Li, A. Habtezion, STING signaling promotes inflammation in experimental acute pancreatitis, Gastroenterology 154 (6) (2018) 1822–1835 e2.
[13] J.M. Romac, R.A. Shahid, S.M. Swain, S.R. Vigna, R.A. Liddle, Piezo1 is a mechanically activated ion channel and mediates pressure induced pancreatitis, Nat. Commun. 9 (1) (2018) 1715.
[14] S.M. Swain, J.M. Romac, R.A. Shahid, S.J. Pandol, W. Liedtke, S.R. Vigna, R. A. Liddle, TRPV4 channel opening mediates pressure-induced pancreatitis initiated by Piezo1 activation, J. Clin. Investig. 130 (5) (2020) 2527–2541.
[15] A. Fazel, J.E. Geenen, K. MoezArdalan, M.F. Catalano, Intrapancreatic ductal pressure in sphincter of Oddi dysfunction, Pancreas 30 (4) (2005) 359–362.
[16] M. Manohar, A.K. Verma, S.U. Venkateshaiah, N.L. Sanders, A. Mishra, Pathogenic mechanisms of pancreatitis, World J. Gastrointest. Pharmacol. Therapeut 8 (1) (2017) 10–25.
[17] L. Wen, T.A. Javed, D. Yimlamai, A. Mukherjee, X. Xiao, S.Z. Husain, Transient high pressure in pancreatic ducts promotes inflammation and alters tight junctions via calcineurin signaling in mice, Gastroenterology 155 (4) (2018) 1250–1263 e5.
[18] N. Shalbueva, O.A. Mareninova, A. Gerloff, J. Yuan, R.T. Waldron, S.J. Pandol, A. S. Gukovskaya, Effects of oxidative alcohol metabolism on the mitochondrial permeability transition pore and necrosis in a mouse model of alcoholic pancreatitis, Gastroenterology 144 (2) (2013) 437–446 e6.
[19] Y. Peng, Y. Yang, Y. Li, T. Shi, N. Xu, R. Liu, Y. Luan, Y. Yao, C. Yin, Mitochondrial (mt)DNA-cyclic GMP-AMP synthase (cGAS)-stimulator of interferon genes (STING) signaling promotes pyroptosis of macrophages via interferon regulatory factor (IRF)7/IRF3 activation to aggravate lung injury during severe acute pancreatitis, Cell. Mol. Biol. Lett. 29 (1) (2024) 61.
[20] M. Chakraborty, A.J. Hickey, M.S. Petrov, J.R. Macdonald, N. Thompson, L. Newby, D. Sim, J.A. Windsor, A.R. Phillips, Mitochondrial dysfunction in peripheral blood mononuclear cells in early experimental and clinical acute pancreatitis, Pancreatology 16 (5) (2016) 739–747.
[21] W.K. Ju, Q. Liu, K.Y. Kim, J.G. Crowston, J.D. Lindsey, N. Agarwal, M.H. Ellisman, G.A. Perkins, R.N. Weinreb, Elevated hydrostatic pressure triggers mitochondrial fission and decreases cellular ATP in differentiated RGC-5 cells, Investig. Ophthalmol. Vis. Sci. 48 (5) (2007) 2145–2151.
[22] L. Tok, M. Naziroglu, A.C. Uguz, O. Tok, Elevated hydrostatic pressures induce apoptosis and oxidative stress through mitochondrial membrane depolarization in PC12 neuronal cells: a cell culture model of glaucoma, J. Recept. Signal Transduct. Res. 34 (5) (2014) 410–416.
[23] J. Kim, H.S. Kim, J.H. Chung, Molecular mechanisms of mitochondrial DNA release and activation of the cGAS-STING pathway, Exp. Mol. Med. 55 (3) (2023) 510–519.
[24] L.E. Newman, G.S. Shadel, Mitochondrial DNA release in innate immune signaling, Annu. Rev. Biochem. 92 (2023) 299–332.

[25] Q. Zhang, M. Raoof, Y. Chen, Y. Sumi, T. Sursal, W. Junger, K. Brohi, K. Itagaki, C. J. Hauser, Circulating mitochondrial DAMPs cause inflammatory responses to injury, Nature 464 (7285) (2010) 104–107.
[26] M.M. Nass, Differential methylation of mitochondrial and nuclear DNA in cultured mouse, hamster and virus-transformed hamster cells. In vivo and in vitro methylation, J. Mol. Biol. 80 (1) (1973) 155–175.
[27] D. Bellizzi, P. D'Aquila, T. Scafone, M. Giordano, V. Riso, A. Riccio, G. Passarino, The control region of mitochondrial DNA shows an unusual CpG and non-CpG methylation pattern, DNA Res. 20 (6) (2013) 537–547.
[28] L.S. Shock, P.V. Thakkar, E.J. Peterson, R.G. Moran, S.M. Taylor, DNA methyltransferase 1, cytosine methylation, and cytosine hydroxymethylation in mammalian mitochondria, Proc. Natl. Acad. Sci. U. S. A. 108 (9) (2011) 3630–3635.
[29] Z. Zhong, S. Liang, E. Sanchez-Lopez, F. He, S. Shalapour, X.J. Lin, J. Wong, S. Ding, E. Seki, B. Schnabl, A.L. Hevener, H.B. Greenberg, T. Kisseleva, M. Karin, New mitochondrial DNA synthesis enables NLRP3 inflammasome activation, Nature 560 (7717) (2018) 198–203.
[30] C. Yan, X. Liu, H. Xu, L. Wang, Cytoplasmic mtDNA clearance suppresses inflammatory immune responses, Trends Cell Biol. 34 (11) (2024) 897–900.
[31] G.A. Ward, R.P. Dalton 3rd, B.S. Meyer, A.F. McLemore, A.L. Aldrich, N.B. Lam, A. H. Onimus, N.D. Vincelette, T.L. Trinh, X. Chen, A.R. Calescibetta, S. M. Christiansen, H.A. Hou, J.O. Johnson, K.L. Wright, E. Padron, E.A. Eksioglu, A. F. List, Oxidized mitochondrial DNA engages TLR9 to activate the NLRP3 inflammasome in myelodysplastic syndromes, Int. J. Mol. Sci. 24 (4) (2023).
[32] M.M. Lin, N. Liu, Z.H. Qin, Y. Wang, Mitochondrial-derived damage-associated molecular patterns amplify neuroinflammation in neurodegenerative diseases, Acta Pharmacol. Sin. 43 (10) (2022) 2439–2447.
[33] J. Chen, S. Liang, C. Li, B. Li, M. He, K. Li, W. Fu, S. Li, H. Mi, Mitochondrial damage causes inflammation via cGAS-STING signaling in ketamine-induced cystitis, Inflamm. Res. 74 (1) (2025) 6.
[34] A. Decout, J.D. Katz, S. Venkatraman, A. Ablasser, The cGAS-STING pathway as a therapeutic target in inflammatory diseases, Nat. Rev. Immunol. 21 (9) (2021) 548–569.
[35] M.J. White, K. McArthur, D. Metcalf, R.M. Lane, J.C. Cambier, M.J. Herold, M. F. van Delft, S. Bedoui, G. Lessene, M.E. Ritchie, D.C. Huang, B.T. Kile, Apoptotic caspases suppress mtDNA-induced STING-mediated type I IFN production, Cell 159 (7) (2014) 1549–1562.
[36] F. Chen, K. Xu, Y. Han, J. Ding, J. Ren, Y. Wang, Z. Ma, F. Cao, Mitochondrial dysfunction in pancreatic acinar cells: mechanisms and therapeutic strategies in acute pancreatitis, Front. Immunol. 15 (2024) 1503087.
[37] M. Bhatia, Inflammatory response on the pancreatic acinar cell injury, Scand. J. Surg. 94 (2) (2005) 97–102.
[38] M.M. Hu, H.B. Shu, Mitochondrial DNA-triggered innate immune response: mechanisms and diseases, Cell. Mol. Immunol. 20 (12) (2023) 1403–1412.
[39] S. Dvorkin, S. Cambier, H.E. Volkman, D.B. Stetson, New frontiers in the cGAS-STING intracellular DNA-sensing pathway, Immunity 57 (4) (2024) 718–730.
[40] A.S. Jahun, F. Sorgeloos, Y. Chaudhry, S.E. Arthur, M. Hosmillo, I. Georgana, R. Izuagbe, I.G. Goodfellow, Leaked genomic and mitochondrial DNA contribute to the host response to noroviruses in a STING-dependent manner, Cell Rep. 42 (3) (2023) 112179.
[41] J.A. Gregg, D.L. Carr-Locke, Endoscopic pancreatic and biliary manometry in pancreatic, biliary, and papillary disease, and after endoscopic sphincterotomy and surgical sphincteroplasty, Gut 25 (11) (1984) 1247–1254.
[42] N. Ebbehoj, L. Borly, P. Madsen, P. Matzen, Comparison of regional pancreatic tissue fluid pressure and endoscopic retrograde pancreatographic morphology in chronic pancreatitis, Scand. J. Gastroenterol. 25 (7) (1990) 756–760.